Biomedicine & Pharmacotherapy 154 (2022) 113590

Contents lists available at ScienceDirect

Biomedicine & Pharmacotherapy

journal homepage: www.elsevier.com/locate/biopha

Curcumin analog JM-2 alleviates diabetic cardiomyopathy inflammation and remodeling by inhibiting the NF-κB pathway

Minxiu Wang [a,b], Leiming Jin [a,b], Qianhui Zhang [b], Weiwei Zhu [b], Hanghui He [b], Shuaijie Lou [b], Wu Luo [b,c], Xue Han [a], Guang Liang [a,b,*]

[a] School of Pharmaceutical Sciences, Hangzhou Medical College, Hangzhou 311399, China
[b] Chemical Biology Research Center, School of Pharmaceutical Sciences, Wenzhou Medical University, Wenzhou 325035, China
[c] Medical Research Center, the First Affiliated Hospital, Wenzhou Medical University, Wenzhou 325035, China

ARTICLE INFO

Keywords:
Diabetic cardiomyopathy
JM-2
Inflammation
NF-κB
Curcumin

ABSTRACT

Cardiac inflammation is an important pathological process in diabetic cardiomyopathy (DCM). Curcumin is a natural compound found in the rhizome of *Curcuma longa* and has been shown to possess multifunctional bioactivities. In the present study, we identified a new curcumin-derived compound, JM-2, and investigated its therapeutic effects against DCM in mouse models of streptozotocin-induced type 1 diabetes mellitus (T1DM) and HFD-induced type 2 diabetes (T2DM). Treatment with JM-2 (10 mg/kg) prevented cardiac functional and structural deficits effectively and reduced cardiac inflammation and fibrosis. JM-2 administration attenuated DCM by inhibiting nuclear factor kappa-B (NF-κB) activation in the heart of both models. In addition, treatment with JM-2 completely prevented the increase in proinflammatory factors and macrophage infiltration in T1DM and T2DM mice. RNA-seq analysis showed that the anti-inflammatory activity of JM-2 was associated with the inhibition of NF-κB activation. In vitro, JM-2 suppressed high glucose (HG)-induced myocardial hypertrophy and fibrosis in H9c2 cells, accompanied by inhibition of HG-induced NF-κB activation. Collectively, our results showed that JM-2, a new curcumin analog, provides strong protection against DCM via inhibition of the NF-κB-mediated inflammation. In summary, our data suggest that the curcumin analog JM-2 may be a potential therapeutic agent for DCM.

1. Introduction

Diabetic cardiomyopathy (DCM) is a diabetes-induced pathophysiological condition that leads to heart failure and cannot be attributed to valvular or ischemic heart disease [1]. Prediabetes is an important risk factor for heart failure (HF). Recently epidemiological have shown that the risk of heart failure was increased in patients with prediabetes [2]. Furthermore, patients with HF and with prediabetes were associated with an increased risk of mortality [3]. The pathological mechanisms underlying DCM are complex, such as mitochondrial dysfunction, oxidative stress, inflammation, apoptosis, autophagy, myocardial fibrosis, and lipo toxicity [4]. Chronic inflammation has emerged as a key pathogenic factor in DCM [5]. Chronic inflammation and upregulated pro-inflammatory factors partially mediate abnormal changes in the diabetic heart [1,6]. Pro-inflammatory cytokines, such as tumor necrosis factor-α (TNFα), interleukin 6 (IL-6), and interleukin 1β (IL-1β),

Abbreviations: ANP, atrial natriuretic peptide; BNP, b-type natriuretic peptide; BSA, bovine serum albumin; CMC-Na, carboxyl methyl cellulose; COL1A1, Collagen Type I Alpha 1 Chain; DAB, diaminobenzidine; DAPI, 4',6-diamidino-2-phenylindole; DCM, diabetic cardiomyopathy; ddH2O, double distilled water; DEPs, differentially expressed proteins; DMEM, Dulbecco's Modified Eagle Medium; EF, ejection fraction; FBS, fetal bovine serum; FITC, fluorescein isothiocyanate; FS, fractional shortening; GAPDH, glyceraldehyde-3-phosphate dehydrogenase; H&E, Hematoxylin and eosin; HF, heart failure; HFD, high-fat diet; HG, high glucose; IL1β, interleukin 1 beta; IL6, interleukin 6; LFD, low-fat diet; LPS, lipopolysaccharide; LVAW s, left ventricular systolic anterior wall thickness; LVAW d, Left ventricular diastolic anterior wall thickness; LVPW s, left ventricular systolic posterior wall thickness; LVPW d, Left ventricular diastolic posterior wall thickness; MTT, methyl thiazolyl tetrazolium; MYH6, Myosin Heavy Chain 6; NF-κB, Nuclear factor kappa-B; OCT, Optimal Cutting Temperature compound; qPCR, quantitative Polymerase Chain Reaction; SDS-PAGE, sodium dodecyl sulfate polyacrylamide gel electrophoresis; T1DM, type 1 diabetes mellitus; T2DM, type 1 diabetes mellitus'; TGFB1, transforming growth factor beta 1; TLRs, Toll-like receptors; TNF-α, tumor necrosis factor-α.WGA, wheat Germ Agglutinin.

* Corresponding author at: School of Pharmaceutical Sciences, Hangzhou Medical University, Hangzhou 311399, China.
E-mail address: wzmcliangguang@163.com (G. Liang).

https://doi.org/10.1016/j.biopha.2022.113590
Received 21 July 2022; Received in revised form 16 August 2022; Accepted 17 August 2022
Available online 31 August 2022

which are associated with hyperglycemia, can induce or exacerbate cardiac injury, leading to further adverse remodeling. Nuclear factor kappa-B (NF-κB) is one of the most important transcription factors involved in proinflammatory gene expression. NF-κB activation has been a common endpoint and inflammatory signaling of cardiac inflammation in diabetes [6,7]. However, owing to the complex pathophysiological mechanisms of DCM, potential effective therapeutic approaches and drugs to prevent and treat this disease are limited. Therefore, it is imperative to develop new drugs for DCM treatment.

Curcumin is the main active component of turmeric, derived from

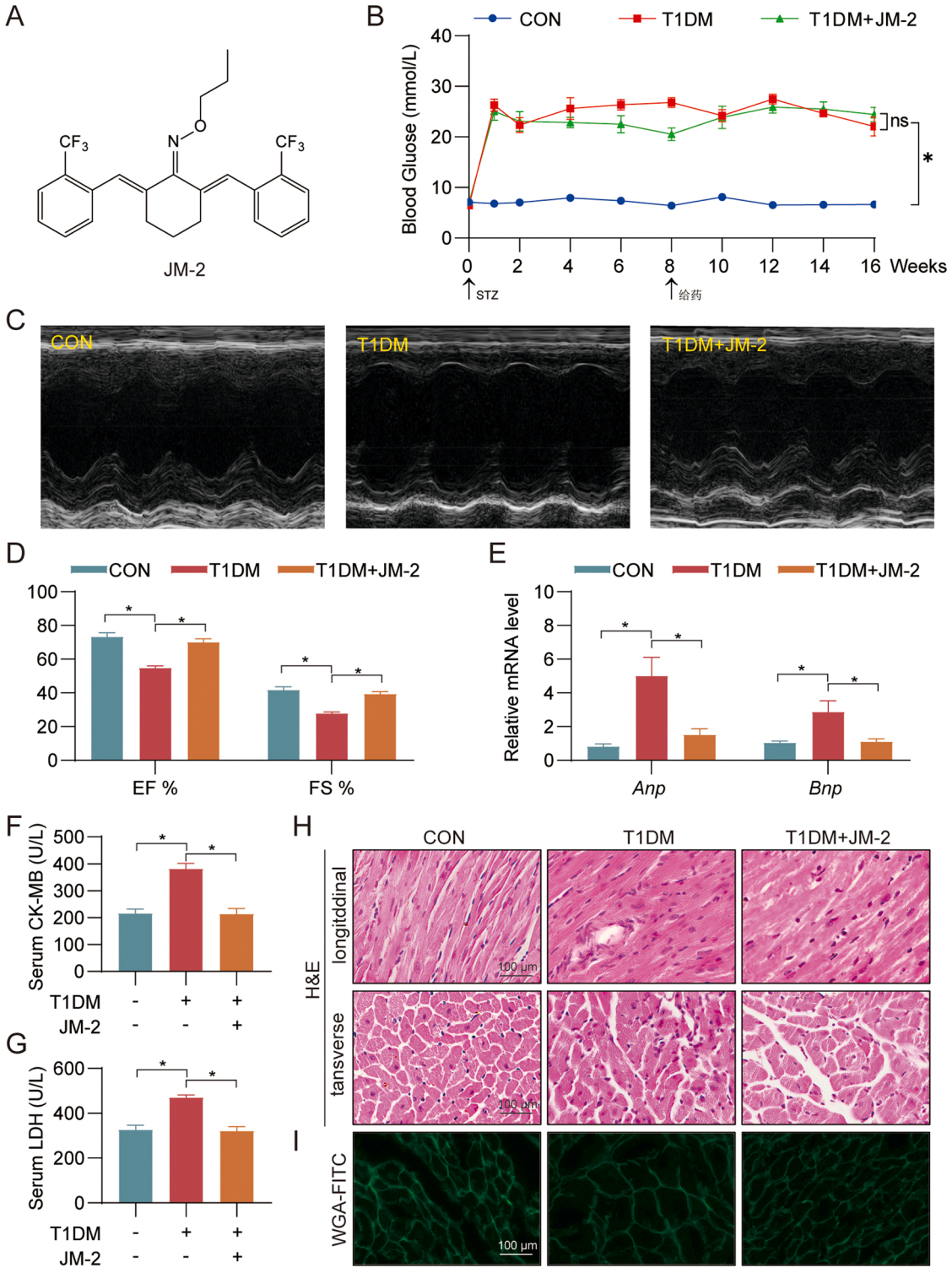

Fig. 1. JM-2 prevented cardiac functional and structural deficits in STZ-induced T1DM mice. (A) The chemical structures of JM-2. (B) Blood glucose levels in mice. (C) Image of non-invasive echocardiography. (D) EF% and FS% of mice were measured by an ultrasonic scanning image system. (E) The mRNA levels of *Anp* and *Bnp* were detected by RT-qPCR in the heart tissues. Transcripts were normalized to *Actb* [n = 6; Mean ± SEM; * , $p < 0.05$]. (F, G) Levels of serum CK-MB (F) and LDH (G) in mice. (H) Representative H&E-stained images of heart tissues showing transverse and longitudinal sections. [scale bar = 100 μm]. (I) Representative WGA-FITC staining images of heart tissues. [scale bar = 100 μm].

the rhizome of the *Curcuma longa* plant [8], and is a multimodal nutraceutical and pharmaceutical agent. Several in vivo and in vitro studies have demonstrated the biological and pharmacological effects of curcumin, including in cardiovascular disease [9], diabetes [10], obesity [11], cancer [12], neurological disorders [13], age-related diseases [14], gastrointestinal disease [15], and rheumatoid arthritis [16]. Previous studies have demonstrated that curcumin treatment significantly ameliorates DCM by regulating myocardial dysfunction and cardiac fibrosis by reducing ROS, apoptosis, and inflammation [17]. Furthermore, several studies have demonstrated that curcumin exhibits anti-inflammation effects by suppressing the NF-κB signaling pathway [18,19]. Curcumin has a wide range of pharmacological effects, but its clinical efficacy is limited owing to its low solubility and bioavailability [20]. Therefore, it is necessary to enhance the biological activity of curcumin by developing curcumin analogs. There are several studies reporting the synthesis of curcumin and its derivatives for cardiovascular applications. Shimizu et al. produced a curcumin analog GO-Y030, which significantly attenuated cardiac hypertrophy and systolic dysfunction in p300-HAT [21]. We have previously reported that a curcumin analog, C66, alleviated DCM [22] and obesity-induced myocardial injury [23] through inhibition of the JNK pathway. Overall, to develop a novel drug for DCM therapy in clinical medication, discovery of novel curcumin analogs that have stronger pharmacological activity than natural curcumin is a promising way.

Recently, we designed and discovered a new curcumin analog, JM-2 (Fig. 1A). Our study found that JM-2 treatment prevented heart inflammation and fibrosis in diabetic mice and inhibited high glucose (HG)-induced inflammatory and fibrotic changes in H9c2 cells. Interestingly, HG-induced inflammatory responses in cardiomyocytes can be completely mitigated by JM-2 treatment. We explored the anti-inflammatory mechanism of JM-2 and identified the NF-κB signaling pathway as the target of JM-2. Our study indicates JM-2 as a new and potential candidate for the treatment of DCM.

2. Materials and Methods

2.1. Antibodies and general reagents

Antibodies against macrophage marker F4/80 (cat# sc-377009) was purchased from Santa Cruz Biotechnology (Dallas, TX, USA). Antibodies against COL-1 (cat# ab34710) and β-MyHC (cat# ab50967) were purchased from Abcam (Cambridge, United Kingdom). Antibodies for IκBα (cat# 4812), phospho-NF-κB p65 (cat# 3033), and NF-κB p65 (cat# 8242) were purchased from Cell Signalling Technology (Danvers, MA, USA). Antibodies against Collagen Type I (Col-1, cat# 14695–1-AP) and TGF-β1 (cat# 21898–1-AP) were purchased from Proteintech (Rosemont, IL, USA). GAPDH antibody (cat# AB-P-R001) was from Hangzhou Goodhere Biotechnology (Hangzhou, China). Horseradish peroxidase-conjugated antibodies were from Beyotime Biotechnology (Shanghai, China).

Pierce ECL Western Blotting Substrate and diaminobenzidine (DAB) were purchased from Thermo Fisher (Waltham, MA, USA). FITC-conjugated wheat-germ agglutinin (WGA-FTIC, cat# GTX01502) was purchased from Gene Tex (San Francisco, CA, USA). Assay kits for Creatine Kinase M and B Isoenzyme Determination Kit (CK-MB, cat# E006–1–1) and Lactate dehydrogenase (LDH, cat# A020–2–2) were purchased from Nanjing Jiancheng Bioengineering Institute (Nanjing, China). Rhodamine-conjugated Phalloidin (Phalloidin-Rho, cat# CA1610–300 T), Masson's Trichrome Stain Kit (cat# 1340), Hematoxylin and eosin (H&E) staining kit (cat# G1120) and Sirius red (cat# S8060) were purchased from Solarbio Life Sciences (Beijing, China). Streptozocin (cat# BJBAG2001) was purchased from Boaigang Biological Technology (Beijing, China).

Compound JM-2 was obtained from our laboratory. JM-2 has a purity of 98.9% and was dissolved in dimethyl sulfoxide (DMSO) for in vitro studies or in 1% sodium carboxyl methyl cellulose (CMC-Na, cat# 419338, Sigma, St. Louis, MO, USA) for in vivo studies.

2.2. Cell culture studies

The immortalized rat cardiomyocyte cell line H9c2 (cat# GNR 5) was obtained from the Shanghai Institute of Biochemistry and Cell Biology (Shanghai, China). H9c2 cells have been widely used as a cardiomyocyte-like cell model for cardiac basic research[24]. The cells were cultured in Dulbecco's modified Eagle medium (DMEM; cat# 11995040, Gibco; Eggenstein, Germany) supplemented with 10% fetal bovine serum (FBS; cat# 14160063, Gibco; Eggenstein, Germany), 1% penicillin/streptomycin (cat# 1514–0122, Invitrogen, Waltham, MA, USA) at 37C in a humidified 5% CO_2 incubator. Cells were cultured in DMEM medium as described above.

2.3. Animal experiments

Mouse studies were initiated following the review and approval of care and experimental procedures by Wenzhou Medical University Animal Policy and Welfare Committee (Approval Document No. wydw2020–0117). All animal experiments conformed to the NIH guidelines (Guide for the care and use of laboratory animals). 36 male C57BL/6 mice weight 18–22 g were obtained from GemPharmatech (Nanjing, China). Male mice were widely used in diabetic models. Mice were housed in a pathogen-free room under 22 ± 2 °C, 50–60% humidity, 12:12 h light-dark cycle. Treatment groups were assigned in a random model.

STZ-induced type 1 diabetic model: streptozotocin (STZ; dissolved in 0.1 mol/L sodium citrate buffer, pH 4.5) was administered intraperitoneally at 50 mg/kg for 5 consecutive days to 7-week-old male C57BL/6 mice (n = 12). Meanwhile six 7-week-old male C57BL/6 mice, as the control group, received the same volume of citrate buffer. Blood glucose levels were measured by a glucometer on day 7. Mice with fasting-blood glucose > 16.6 mM were selected and considered as diabetic. The control mice (n = 6) received the same volume of citrate buffer. All mice were fed with water and standard rodent diet. At 9th week after diabetes was onset, 12 diabetic animals were randomly divided into two groups: T1DM (n = 6), and JM-2 (10 $mg{\cdot}kg^{-1}$ per day)-treated T1DM (T1DM+JM-2, n = 6). In the JM-2-treated groups, JM-2 (10 mg/kg) was administered as oral gavage once every 2 days for another 8 weeks (from 9th to 16th week), respectively. The vehicle used for JM-2 administration is 1% CMC-Na solution. The T1DM group and age-matched control group (n = 6) received 1% CMC-Na solution alone according to the same schedule.

High-fat-diet (HFD)-induced diabetic model[25]: Eighteen male C57BL/6 mice were randomly divided into three groups: low-fat diet (LFD), high-fat diet (HFD) and 10 $mg{\cdot}kg^{-1}$ twice a day JM-2-administered HFD mice (HFD+JM-2). Each group had n = 6. LFD consisted of 10 kcal.% fat, 20 kcal.% protein, and 70 kcal.% carbohydrate (MediScience Diets Co., Ltd., Yangzhou, China; cat. #MD12031). HFD consisted of 60 kcal.% fat, 20 kcal.% protein, and 20 kcal.% carbohydrates (cat. #MD12033). Mice were fed these diets for 24 weeks. In the JM-2-treated groups, JM-2 (10 mg/kg) was administered as oral gavage once every 2 days for another 8 weeks (from 16th to 24th week), while the HFD group and LFD group received the same volume of diluent (1% CMC-Na solution) in the same schedule.

No mice died during the experiment. Body weight and blood glucose levels were recorded weekly. At the end of treatment, mice were sacrificed under anesthesia. Blood and Heart tissues were collected after the study. Serum myocardial lactate dehydrogenase (LDH) and creatine kinase-cardiac (CK-MB) levels were detected and analyzed as the main laboratory indicators related to heart injury. The transcript levels of Atrial natriuretic peptide (ANP) and B-type natriuretic peptide (BNP) in heart tissue were detected by real-time qPCR assay. Heart tissues were snap-frozen in liquid nitrogen for gene and protein expression analyses or fixed with 4% paraformaldehyde for histological analysis.

2.4. Cardiac functional tests

Systolic and diastolic cardiac function was determined non-invasively via transthoracic echocardiography in anesthetized mice, one day before the sacrifice as described previously[26]. ACUSON Oxana2 ultrasonic diagnostic apparatus (Siemens Medical Solutions Inc., CA, USA) equipped with a VTIQ mode and a 9L4 linear array transducer (7–9 MHz) were used. Ejection fraction (EF%) was calculated from LV end-diastolic volume (LVEDV) and end-systolic volume (LVESD) using the equation of (LVEDV–LVESV)/LVEDV × 100). Fractional shortening (FS) was calculated using the equation (FS% = [(LVIDd–LVIDs)/LVIDd] × 100).

2.5. Heart tissue staining

Heart tissues were fixed in 4% paraformaldehyde, embedded in paraffin, and sectioned at 5-μm thickness. After dehydration, sections were stained with hematoxylin and eosin (H&E). Stained sections were evaluated for general histopathological damage using light microscopy. Additional paraffin sections were stained with Sirius Red and Masson's Trichrome Stain to assess heart fibrosis.

For immunohistochemistry, sections were deparaffinized, hydrated and subjected to heat-induced antigen retrieval (0.01 M sodium citrate buffer, pH = 6.0). Slides were blocked with 3% hydrogen peroxide for 30 min and in 1% BSA for 30 min and incubated with F4/80 antibodies (1:200) overnight at 4 °C. Horseradish peroxidase (HRP)-labeled secondary antibodies were then applied for 1 h at 37 °C. Immunoreactivity was detected by diaminobenzidine (DAB). Slides were counterstained with hematoxylin. Images were acquired using a Nikon microscope (Nikon, Japan). Image J analysis software version 1.53i (NIH; Bethesda, MD, USA) was used to determine staining-positive cells.

Immunofluorescence staining of liver tissues was performed using frozen tissues in Optimal Cutting Temperature (OCT) media. The outline of myocardial cells was demarcated by wheat Germ Agglutinin-fluorescein isothiocyanate (WGA-FTIC) staining. 5-μm thick frozen sections were permeabilized. WGA-FITC dye solution (1:200) was added and dyed for 30 min at 37 °C. Sections were counterstained with DAPI and imaged using an epi-fluorescence microscope (Nikon, Japan).

2.6. Rhodamine phalloidin staining

To assess the hypertrophic changes, H9c2 cells were fixed with 4% paraformaldehyde, permeabilized with 0.1% Triton X-100, and stained with rhodamine-conjugated phalloidin (Phalloidin-Rho) at a concentration of 50 ng/ml for 30 min. Sections were counterstained with DAPI and imaged using an epi-fluorescence microscope (Nikon, Japan).

2.7. Western blot and immunoprecipitation

Cell and tissue lysates were prepared in RIPA buffer (cat# P0013B; Beyotime Biological Technology, Shanghai, China) and protein concentration was measured. Protein lysates were separated by sodium dodecyl sulfate-polyacrylamide gel electrophoresis and transferred to polyvinylidene fluoride membranes. Membranes were blocked in Tris-buffered saline (pH 7.4, containing 0.05% Tween 20% and 5% non-fat milk) for 1 h at room temperature and incubated with primary antibodies at 4 ℃ overnight. Secondary antibodies were applied for 1 h at room temperature. Immunoreactivity was visualized using enhanced chemiluminescence reagent (Bio-Rad) and quantified using Image J analysis software version 1.53i. Values were normalized to respective housekeeping proteins.

2.8. Real-time qPCR

mRNA levels were detected by real-time qPCR. Total RNA was extracted from cells and tissues using Trizol Reagent (cat# 9109, Takara Bioscience, Ann Arbor, MI). RNA was reverse-transcribed using PrimeScript RT reagent (cat# RR047A, Takara Bioscience, Ann Arbor, MI). Real-time PCR was subsequently conducted using TB Green Premix Ex Taq II (cat#RR820A, Takara Bioscience, Ann Arbor, MI) on CFX96 Touch Real-Time PCR Detection System (Bio-Rad). Relative expression was calculated by $2^{\Delta\Delta}$Ct method with *Actb* normalization. Primer sequences are listed in Supplementary Table S1.

2.9. MTT assay

H9c2 cells were seeded in 96-well plates at 3000 cells per well and cultured overnight to allow adherence. Cells were then exposed to JM-2 at increasing concentrations, including 0.05, 0.5, 1, 2.5, 5, 10, 20, and 50 μM. Control cells received DMSO as a vehicle. After 24-h incubation, methyl thiazolyl tetrazolium (MTT, cat# M8180–250MG, Solarbio, Beijing, China) was added to each well. Cells were incubated for 4 h and then DMSO was added. Absorbance was measured at 570 nm using SpectraMax M5 microplate reader (Molecular Devices, CA, USA). Cell viability was expressed as the percentage of control.

2.10. Statistical analysis

All experiments are randomized and blinded. All data are reported as Mean ± SEM. Statistical analysis was performed with GraphPad Prism 8.0 software (San Diego, CA, USA). We used one-way ANOVA followed by Dunnett's post hoc test when comparing more than two groups of data and one-way ANOVA, nonparametric Kruskal–Wallis test, followed by Dunnett's post hoc test when comparing multiple independent groups. P values less than 0.05 were considered to be statistically significant. Post-tests were run only if F achieved $P < 0.05$ and there was no significant variance inhomogeneity.

3. Results

3.1. JM-2 prevented cardiac functional and structural deficits in STZ-induced T1DM mice

To examine the pharmacological effects of JM-2, STZ was used to induce DCM in a mouse model. We induced T1DM in 7-week-old male C57BL/6 mice using STZ and treated the mice with JM-2 (10 mg/kg) for 16 weeks. JM-2 did not change body weight or fasting blood glucose levels in the mice (Fig. S1A, Figure1B). We demonstrated the protective effect of JM-2 on heart function using non-invasive echocardiography for assessment. JM-2 also effectively abolished STZ-induced cardiac dysfunction, as evidenced by the reversed ejection fraction (EF) % and fractional shortening (FS) % values in JM-2–treated T1DM mice (Fig. 1C–1D, Table 1). ANP and BNP are standard biomarkers of heart failure[27,28]. The mRNA levels of ANP and BNP were increased in T1DM mice. However, this increase was not seen in JM-2–treated mice

Table 1
Biometric and echocardiographic measurements in STZ-induced T1DM mice.

Parameters	CON n = 6	T1DM n = 6	T1DM+JM-2 n = 6
EF%	73.35 ± 2.37	54.90 ± 1.18 * *	70.57 ± 1.62$^{\#\#}$
FS%	41.78 ± 1.89	27.88 ± 0.81 * *	39.41 ± 3.94$^{\#\#}$
LVAW;s(MM)	1.44 ± 0.11	1.14 ± 0.09 *	1.45 ± 0.08$^{\#}$
LVAW;d(MM)	0.84 ± 0.11	0.74 ± 0.09	0.85 ± 0.08
LVPW;s(MM)	1.44 ± 0.06	1.33 ± 0.19	1.48 ± 0.11
LVPW;d(MM)	0.94 ± 0.08	0.97 ± 0.15	1.17 ± 0.08

Transthoracic echocardiography was performed on mice at the end of the animal study; EF, ejection fraction; FS, fractional shortening; LVAW;s, left ventricular systolic anterior wall thickness; LVAW;d, Left ventricular diastolic anterior wall thickness; LVPW;s, left ventricular systolic posterior wall thickness; LVPW;d, Left ventricular diastolic posterior wall thickness. Data presented as mean ± SEM. n = 6 per group; *$p < 0.05$, * *$p < 0.01$ compared with CON group; $^{\#}p < 0.05$, $^{\#\#}p < 0.01$ compared with T1DM.

with T1DM (Fig. 1E). Treatment with JM-2 reduced the serum levels of LDH and CK-MB in T1DM mice (Fig. 1F–G). These data suggest that JM-2 treatment prevented heart damage in mice with T1DM. Next, we examined the effects of JM-2 on cardiac morphological impairment. Analysis of the harvested heart tissues by H&E and WGA staining showed structural and hypertrophic changes in T1DM mice but not in mice treated with JM-2 (Fig. 1H–I, Fig. S1B). These results indicated that JM-2 protects T1DM mice from alterations in cardiac function and structural deficits.

3.2. JM-2 prevents STZ-induced heart fibrosis in mice

Cardiac fibrosis and inflammation are important pathological processes in STZ-induced heart failure, prompting us to investigate whether JM-2 prevents heart fibrosis in T1DM mice. The heart tissues of mice were stained using Picrosirius Red and Masson's trichrome. Staining with Picrosirius Red (Fig. 2A–D) and Masson's trichrome (Fig. 2E–H) also showed the suppressive activity of JM-2 on fibrotic responses in T1DM mice. The protein and mRNA levels of fibrosis-associated factors Myosin heavy chain (MyHc), Collagen type I (Col-1), and transforming growth factor (TGF-β)) confirmed the protective role of JM-2 in T1DM (Fig. 2I–K). These results show increased fibrosis responses in mice with T1DM, but not in JM-2–treated mice.

3.3. JM-2 prevented cardiac functional and structural deficits in HFD-induced diabetes mellitus (T2DM) mice

To evaluate the effect of JM-2 on T2DM, we performed the same studies in mice with HFD-induced diabetes. We reasoned that JM-2 might have a similar effect in T2DM. We fed 8-week-old male C57BL/6 mice an HFD for 24 weeks and examined their heart function. JM-2 did not change the body weight or blood glucose levels in T2DM mice, similar to that observed in STZ-induced T1DM mice (Fig. 3A, Fig. S2A). Assessment of heart function revealed similar protection by JM-2 as seen in the STZ-induced T1DM mouse model (Fig. 3B–C, Table 2). Consistently, treatment with JM-2 did not increase the mRNA levels of ANP or BNP in T2DM mice (Fig. 3D). To ascertain that JM-2 prevents alterations in cardiac injury, we measured the serum levels of LDH and CK-MB and observed that the JM-2 treatment group had low levels of LDH and CK-MB (Fig. 3E–F). Concurrently, analysis of the harvested heart tissues by H&E and WGA staining showed structural and hypertrophic changes in HFD-induced T2DM mice, but not in mice treated with JM-2 (Fig. 3G–H, Fig. S2B). Collectively, these results indicated that JM-2 protects HFD-induced T2DM mice from alterations in cardiac function and structural deficits.

3.4. JM-2 prevents heart fibrosis in HFD-induced T2DM mice

A previous study showed that a high-fat diet can induce heart

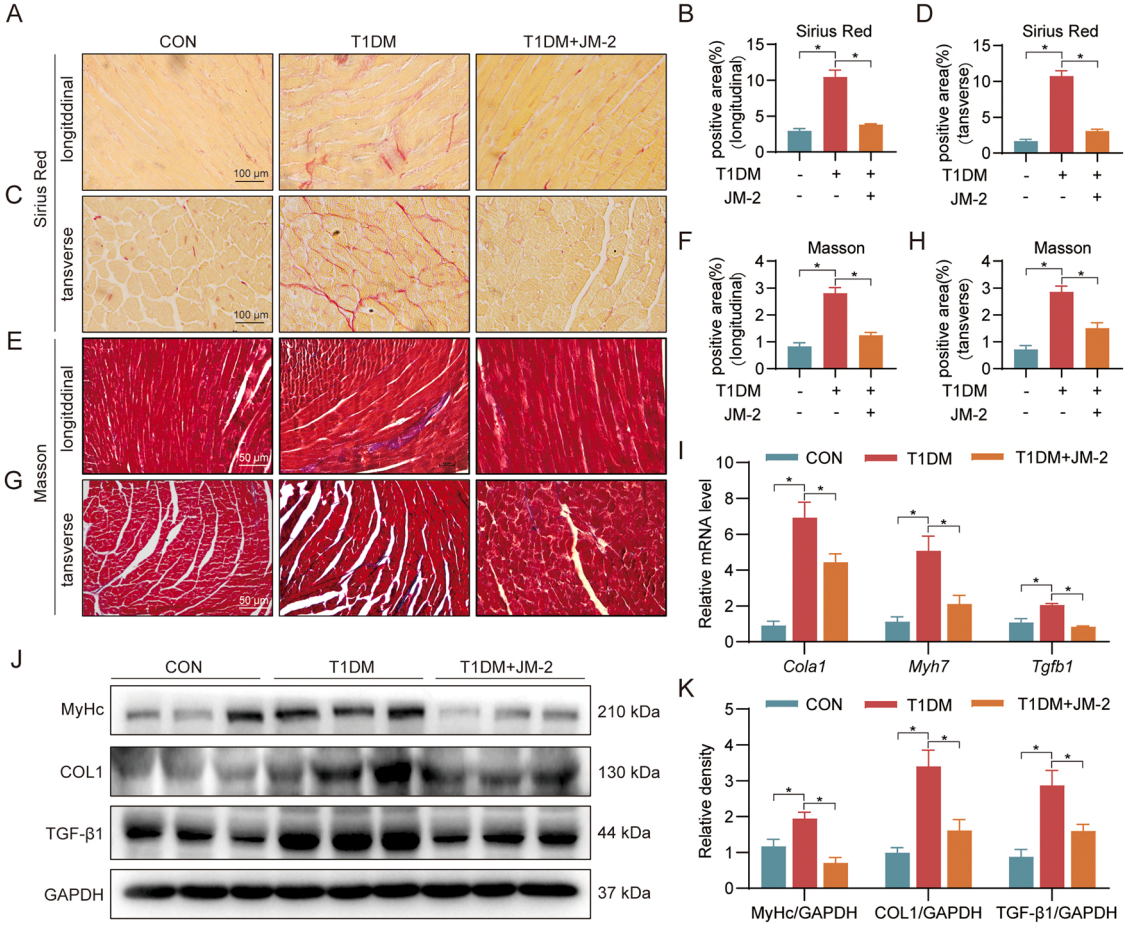

Fig. 2. JM-2 prevents STZ-induced heart fibrosis in mice. (A-D) Representative Picro Sirius Red-stained images of heart tissues and quantification of perivascular fibrotic areas (%) showing longitudinal and transverse sections. [scale bar = 100 μm]. (E-H) Representative Masson's Trichrome-stained images of heart tissues and quantification of perivascular fibrotic areas (%) showing longitudinal and transverse sections. [scale bar = 50 μm]. (I) The mRNA levels of *Col1a1, myh7,* and *Tgfb1* were detected by RT-qPCR in the heart tissues. Transcripts were normalized to *Actb* [n = 6; Mean ± SEM; * , $p < 0.05$]. (J-K) Measurement of fibrosis-related proteins (MyHc, Col1, and TGF-β1) in heart tissue lysates. Representative immunoblots (J) and densitometric quantification (K) are shown. GAPDH was used as control.

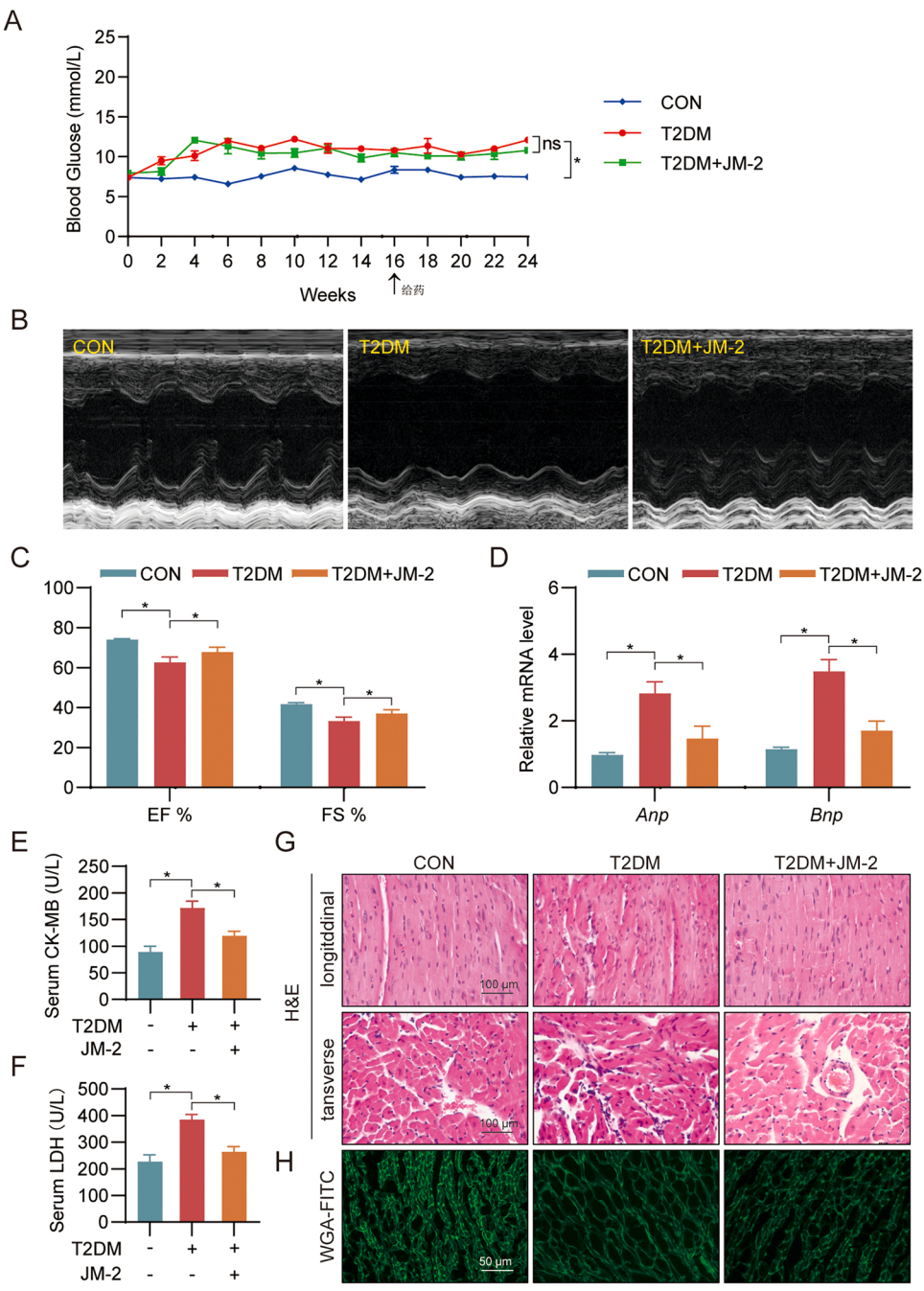

Fig. 3. JM-2 prevented cardiac functional and structural deficits in HFD-induced diabetes mellitus (T2DM) mice. (A) Blood glucose levels in mice. (B) Image of non-invasive echocardiography. (C) EF% and FS% of mice were measured by an ultrasonic scanning image system. (D) The mRNA levels of *Anp* and *Bnp* were detected by RT-qPCR in the heart tissues. Transcripts were normalized to *Actb* [n = 6; Mean ± SEM; *, $p < 0.05$]. (E, F) Levels of serum CK-MB (E) and LDH (F) in mice. (G) Representative H&E-stained images of heart tissues showing transverse and longitudinal sections. [scale bar = 100 μm]. (H) Representative WGA-FITC staining images of heart tissues. [scale bar = 50 μm].

fibrosis. Next, we sought to identify the effects of JM-2 on T2DM heart fibrosis. Similar to our results in T1DM mice, Masson's trichrome (Fig. 4A–D) and Picrosirius red staining (Fig. 4E–H) analyses showed that the increased collagen deposition in the hearts was also substantially improved in JM-2–treated mice, which was confirmed by gene markers of hypertrophy and fibrosis (MyHc, Col1, and TGF-β) (Fig. 4I, Fig. S3A). These data indicate that JM-2 prevents heart fibrosis in HFD-induced T2DM mice.

3.5. *JM-2 prevents heart inflammation in STZ-induced T1DM and HFD-induced T2DM mice by inhibiting the NF-κB pathway*

To identify the potential mechanism of the protective activity of JM-2 against STZ-induced heart injury, we performed RNA sequencing analysis using mouse heart tissues. A total of 420 significantly different genes were found, including 441 upregulated and 201 downregulated genes (Fig. S4A–S4B) when comparing the JM-2 +T1DM group to the T1DM group. We performed KEGG enrichment analysis of these altered genes. We found that the NF-κB signaling pathway was present and ranked among the top ten pathways altered between the JM-2 +T1DM and T1DM groups. This indicated the involvement of NF-κB in the cardiac protection of JM-2 in this model (Fig. 5A). Based on these results, we probed heart tissue lysates for the phosphorylated (p-) p65 subunit of NF-κB. We also measured the levels of the inhibitor of κB as a measure of NF-κB activity. Our results showed a noticeably increased phosphorylated (p)-p65 and reduced IκB levels in lysates prepared from T1DM mice compared to these in JM-2–treated mice (Fig. 5B, Fig. S4C). We also observed similar changes in the HFD-induced T2DM model (Fig. 5C, Fig. S4D). In addition, treatment with JM-2 in T1DM and T2DM mice not only strongly reduced the basal activation of NF-κB, but also nearly

Table 2
Biometric and echocardiographic measurements in HFD-induce T2DM mice.

Parameters	CON n = 6	T2DM n = 6	T2DM+JM-2 n = 6
EF%	74.05 ± 0.53	62.62 ± 2.71 * *	67.92 ± 2.40$^{\#\#}$
FS%	41.80 ± 0.57	33.25 ± 1.95 * *	37.15 ± 1.79$^{\#\#}$
LVAW;s(MM)	1.62 ± 0.07	1.74 ± 0.14	1.71 ± 0.10
LVAW;d(MM)	1.07 ± 0.08	1.32 ± 0.13 *	1.15 ± 0.08$^{\#}$
LVPW;s(MM)	1.57 ± 0.08	1.37 ± 0.15	1.40 ± 0.07
LVPW;d(MM)	1.20 ± 0.12	1.09 ± 0.17	1.15 ± 0.12

Transthoracic echocardiography was performed on mice at the end of the animal study; EF, ejection fraction; FS, fractional shortening; LVAW;s, left ventricular systolic anterior wall thickness; LVAW;d, Left ventricular diastolic anterior wall thickness; LVPW;s, left ventricular systolic posterior wall thickness; LVPW;d, Left ventricular diastolic posterior wall thickness. Data presented as mean ± SEM. n = 6 per group; *p < 0.05, * *p < 0.01 compared with CON group; $^{\#}$p < 0.05, $^{\#\#}$p < 0.01 compared with T2DM.

completely prevented the increase in downstream NF-κB and inflammatory factors (Fig. 5D–E). Complementarily, we also found cytokine-cytokine receptor interactions and chemokine signaling pathways in the KEGG enrichment analysis. Immunohistochemical staining showed that compared to hearts of control mice, the hearts from T1DM and obese mice had significantly increased F4/80 immunoreactivity (Fig. 5F-I). These studies showed that macrophage infiltration was increased in T1DM and T2DM cardiac tissues. In contrast, treatment with JM-2 almost completely abrogated the increase in macrophage infiltration. These studies suggest that JM-2 suppresses STZ- and HFD-induced cardiomyocyte injury by inhibiting the NF-κB pathway.

3.6. *JM-2 attenuates HG-induced hypertrophy and fibrosis via inhibiting inflammation responses in H9c2 cells*

To evaluate whether JM-2 could suppress the effects of HG on cardiac cells, we used cultured H9c2 cells as a cellular model. The MTT assay showed that JM-2, at concentrations ranging from 0.05 to 50 μM, did not show significant toxicity in H9c2 cells (Fig. S5A). The IC_{50} of JM-2 for H9c2 cells was > 176.2 μM; thus, we chose 10 μM (≈1/20 IC_{50}) for the in vitro study. We then continuously treated H9c2 cells with JM-2 at 10 μM for 1 h before exposure to HG (33 mM glucose). We confirmed

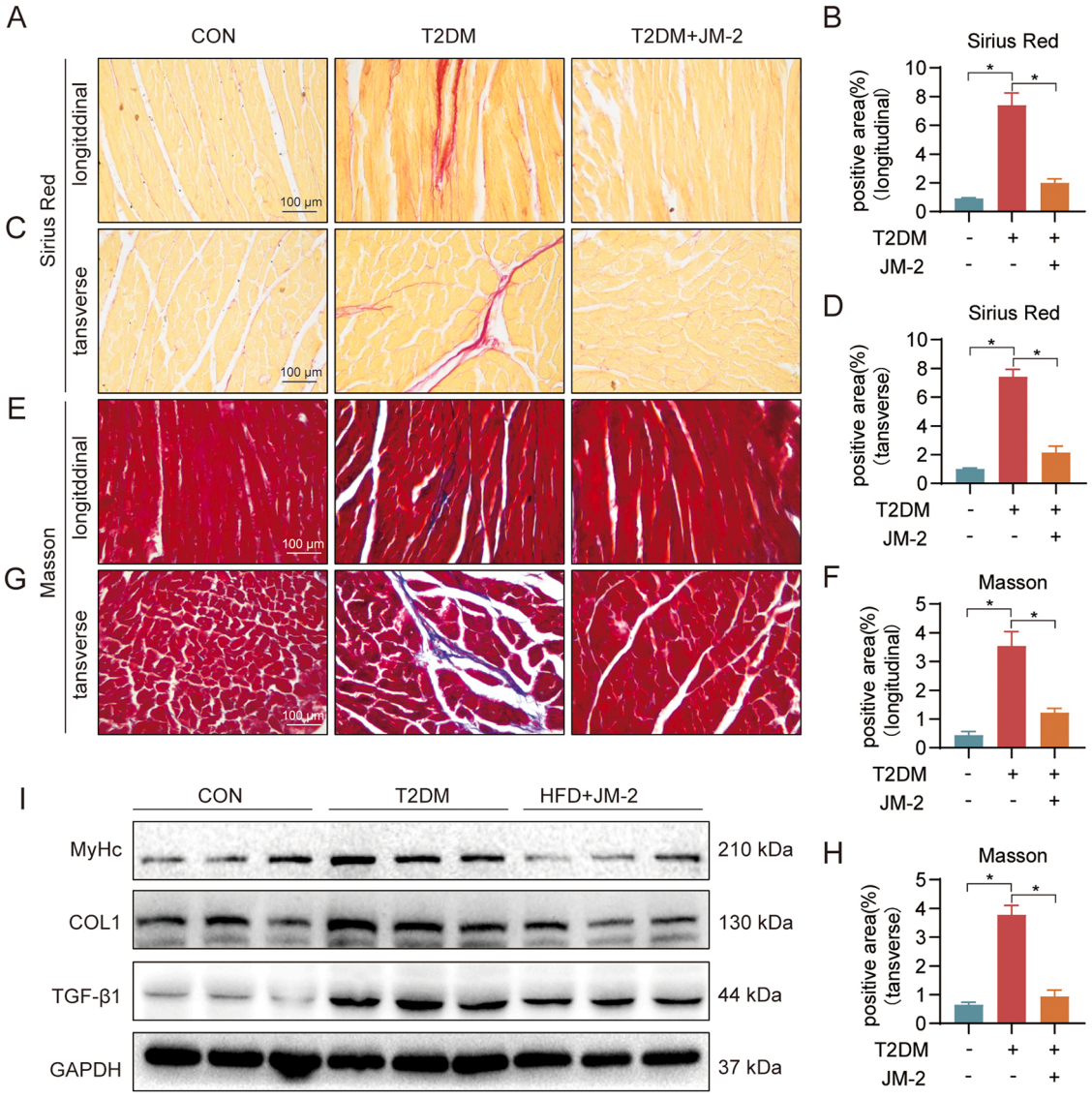

Fig. 4. JM-2 prevents heart fibrosis in HFD-induced T2DM mice. (A-D) Representative Picro Sirius Red-stained images of heart tissues and quantification of perivascular fibrotic areas (%) showing longitudinal and transverse sections. [scale bar = 100 μm]. (E-H) Representative Masson's Trichrome-stained images of heart tissues and quantification of perivascular fibrotic areas (%) showing longitudinal and transverse sections. [scale bar = 100 μm]. (I) Measurement of fibrosis-related proteins (MyHc, Col1, and TGF-β1) in heart tissue lysates. Representative immunoblots are shown. GAPDH was used as control.

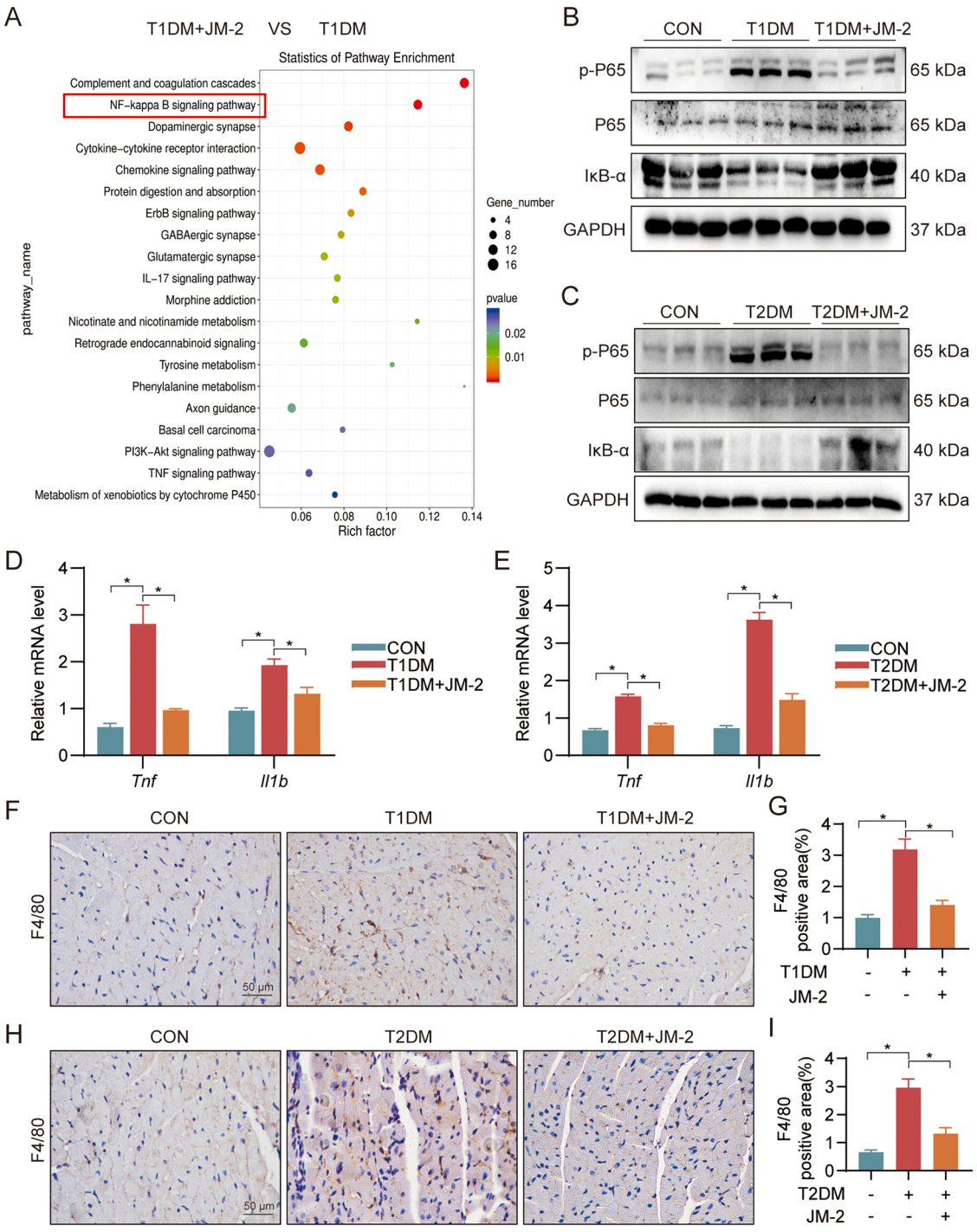

Fig. 5. JM-2 prevents heart inflammation in STZ-induced T1DM and HFD-induced T2DM mice by inhibiting the NF-κB pathway. (A) KEGG enrichment of the differential gene in T1DM+JM-2 group vs. T1DM group. (B) Immunoblot analysis of NF-κB p65, and IκBα in T1DM heart tissues. Phosphorylated proteins and total proteins were measured [Mean ± SEM; n = 6; * , $p < 0.05$]. (C) Immunoblot analysis of NF-κB p65, and IκBα in T2DM heart tissues. Phosphorylated proteins and total proteins were measured [Mean ± SEM; n = 6; * , $p < 0.05$]. (D) The mRNA levels of *Tnf* and *Il1b* were detected by RT-qPCR in the T1DM heart tissues. Transcripts were normalized to *Actb* [n = 6; Mean ± SEM; * , $p < 0.05$]. (E) The mRNA levels of *Tnf* and *Il1b* were detected by RT-qPCR in the T2DM heart tissues. Transcripts were normalized to *Actb* [n = 6; Mean ± SEM; * , $p < 0.05$]. (F-G) Staining of T1DM heart tissues of mice for macrophage marker F4/80. Sections were counterstained with hematoxylin (blue). Quantification of the immunoreactive area is shown in panel G. [scale bar = 50 μm]. (H-I) Staining of T2DM heart tissues of mice for macrophage marker F4/80. Sections were counterstained with hematoxylin (blue). Quantification of the immunoreactive area is shown in panel I. [scale bar = 50 μm].

cardiomyocyte hypertrophy by staining H9c2 cells with rhodamine-phalloidin to measure the cell size. Rhodamine phalloidin staining showed that cell size increased with exposure to HG, whereas this increase was reversed in cells pretreated with JM-2 (Fig. 6A–B). The mRNA and protein markers of fibrosis (MyHc, Col1, and TGF-β) increased following the exposure of H9c2 cells to HG for 12 h. However, cells pretreated with JM-2 did not exhibit the same response (Fig. 6C–D, Fig. S5B). Moreover, immunoblotting assay for the p-p65 subunit of NF-κB, inhibitor of κB (IκB-α) (Fig. 6E–F,Fig. S5C), and staining assay for the p65 subunit of NF-κB (Fig. 6G, Fig. S4C) confirmed that JM-2

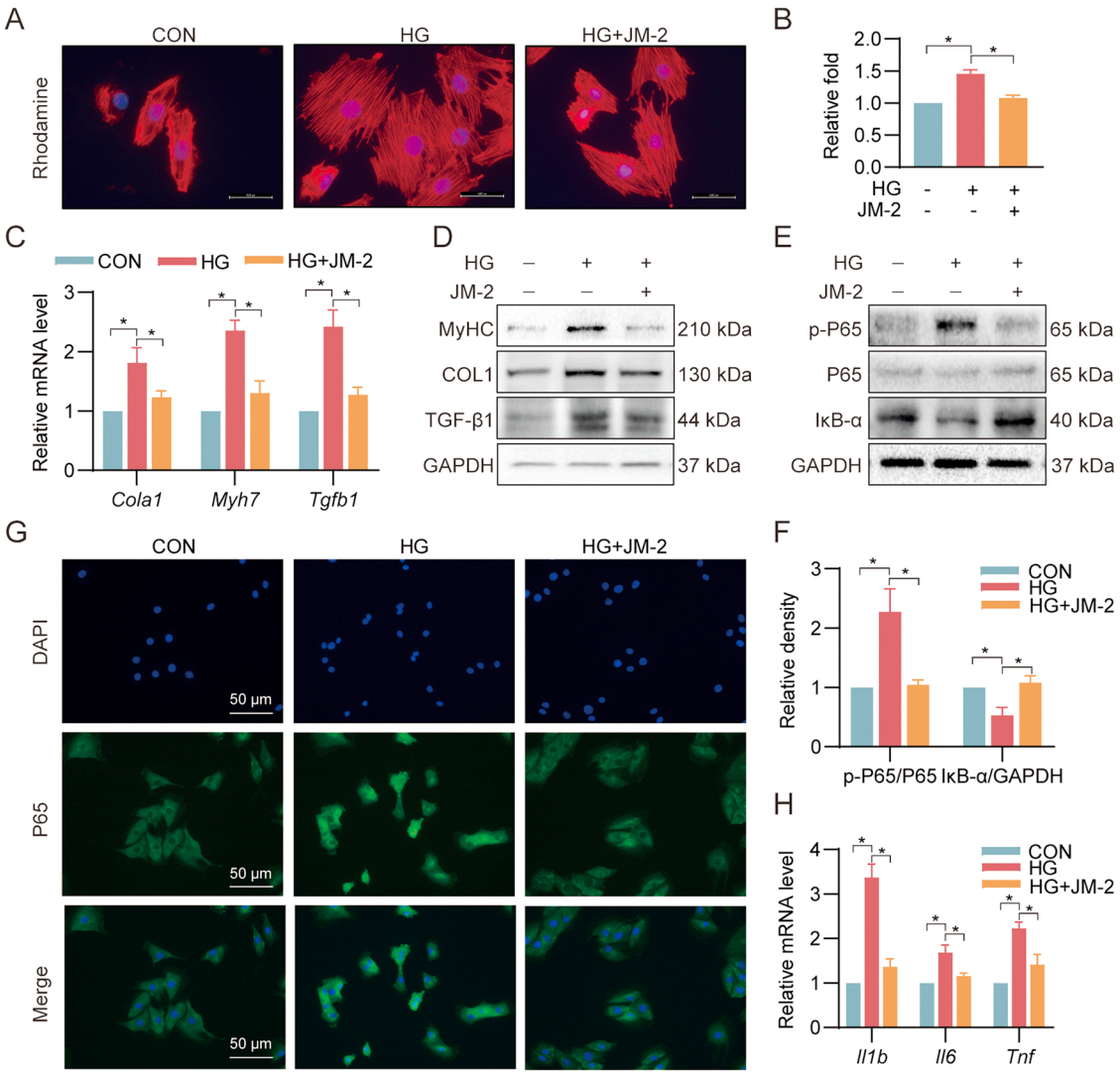

Fig. 6. JM-2 attenuates HG-induced hypertrophy, fibrosis, and inflammation responses in H9C2 cells. JM-2 prevents HG-induced hypertrophy, fibrosis, and inflammation in H9c2 cells. H9c2 cells were pretreated with 10 μM JM-2 for 1 h and then exposed to HG (33 mM) for 12 or 24 h. Protein and RNA were extracted to perform immunoblotting and qPCR respectively. (A-B) TRITC phalloidin (red) staining of H9c2 cells showing the effect of JM-2 on HG-induced hypertrophic responses. Slides were counterstained with DAPI (blue). (C) The mRNA levels of *Col1a1, myh7,* and *Tgfb1* were detected by RT-qPCR in H9C2 cells. Transcripts were normalized to *Actb* [n = 3; Mean ± SEM; * , $p < 0.05$]. (D) Measurement of fibrosis-related proteins (MyHc, Col1, and TGF-β1) in H9c2 cell lysates. Representative immunoblots are shown. GAPDH was used as control. [n = 3; Mean ± SEM; * , $p < 0.05$]. (E-F) Immunoblot analysis of NF-κB p65, and IκBα in H9c2 cells. Phosphorylated proteins and total proteins were measured [n = 3; Mean ± SEM; * , $p < 0.05$]. (G) H9c2 cells were pretreated with 10 μM JM-2 for 1 h and then exposed to HG (33 mM) for 1 h. Cells were stained p65 subunit of NF-κB (Green). Cells were counterstained with DAPI (blue). [scale bar = 50 μm]. (H) The mRNA levels of *Il1b, Il6, and Tnf* were detected by RT-qPCR in H9C2 cells. Transcripts were normalized to *Actb* [n = 3; Mean ± SEM; * , $p < 0.05$].

pretreatment suppressed HG-induced NF-κB activation in H9c2 cells. The mRNA levels of proinflammatory factors (*Il1b, Tnf*, and *Il6*) were significantly reduced in JM-2–treated cells exposed to HG (Fig. 6H). These data suggest that JM-2 reduced HG-induced hypertrophy, fibrosis, and inflammation in cardiomyocytes.

4. Discussion

In the present study, we examined the potential therapeutic effects of the curcumin analog JM-2 in DCM. Our study demonstrated the protective effect of JM-2 on STZ- and obesity-induced cardiac hypertrophy, fibrosis, dysfunction, and inflammation. HG activated the NF-κB signaling pathway in both HG-treated cardiomyocytes and in T1DM and T2DM mouse hearts. Owing to NF-κB activation, the expression of inflammatory cytokine (Tnf, Il6, and Il1β) genes was increased, which aggravated heart fibrosis and dysfunction. All these processes were significantly reversed by JM-2 treatment. Overall, JM-2 provided cardioprotection against cardiac dysfunction in both type 1 and type 2 diabetic mice.

We found that the body weight of the JM-2–treated group was significantly lower than that of the model group in obesity-induced type 2 diabetic mice. Obesity-induced type 2 diabetes is correlated with the development of islet inflammation and systemic low-grade inflammation[29]. Based on this mechanism, we speculate that JM-2 may alleviate islet and systemic inflammation by inhibiting the NF-κB signaling pathway. In addition, we speculate that the curcumin analog JM-2 may alleviate type 2 diabetes or other obesity diseases through lipid metabolism. Curcumin has been shown to have protective effects against obesity and metabolic diseases. Panzhinskiy et al. showed that curcumin exhibited a positive effect in reducing weight gain and adiposity in response to high-fat feeding[30]. Baziar et al. showed that curcumin might have a positive effect on visceral fat and abdominal obesity associated with Non-alcoholic fatty liver disease[31]. These studies indicate that our curcumin analog, JM-2, exhibits the same

pharmacological activity as curcumin in targeting weight and lipid metabolism. In future, we plan to explore other pharmacological effects.

A typical proinflammatory element with determined activity in the transcription of multiple inflammatory cytokines, NF-κB is highly active in the inflammation pathology of DCM[32–34]. These inflammatory cytokines may affect myocardial metabolic processes and interfere with cardiomyocyte contractile properties, aggravating the development of DCM. Simultaneously, NF-κB inhibition is thought to be the key mechanism underlying the anti-inflammatory action of curcumin[35]. Several reports have demonstrated the powerful ability of curcumin to inhibit NF-κB in the treatment of numerous diseases such as ulcerative colitis[36], acute kidney injury[37], and lipopolysaccharide (LPS)-induced neuroinflammation[38]. In addition, our RNA-sequencing analysis showed that the NF-κB pathway was downregulated by JM-2 treatment in vivo. This consistent phenomenon indicated that the major bioactive fragments of curcumin were retained during the conversion process from curcumin to JM-2.

There are a few unanswered but important questions in our study which warrant future investigations. Firstly, how does JM-2 inhibit the NF-κB signaling pathway? Based on previous studies, the answer to this question may be related to Toll-like receptors (TLRs). Activation of TLRs initiates a signal transduction cascade that culminates in activation of the NF-κB transcription factor[39]. Toll-like receptor 4 regulates inflammation and has been linked to the pathogenesis of heart disease, which is upregulated in DCM[40]. Toll-like receptor 4 is considered a strong inflammatory stimulator that can activate the NF-κB signaling pathway. Stimulation of TLR4 further activates the NF-κB pathway, which plays an important role in DCM inflammation. Previous studies have shown that curcumin attenuates inflammation by inhibiting TLR4. Zhang et al. showed that curcumin attenuated the activation of the TLR4/NF-κB pathway and downregulation of TREM2 expression in LPS-activated BV2 cells[38]. In addition, curcumin attenuates renal interstitial fibrosis by inhibiting the TLR4/NF-κB and PI3K/AKT signaling pathways[41]. Based on these studies, we speculated that the curcumin analog JM-2 may further inhibit the activation of NF-κB by modulating the activation of TLR4. Therefore, future studies are needed to elucidate the mechanism by which JM-2 inhibits the NF-κB signaling pathway. Secondly, it's our limitation that we exposed cardiomyocytes in single high glucose to mimic the pathophysiological changing of T1DM in vitro studies. To simulate the physiological environment of T2DM, HG plus palmitic acid (PA) was usually used as stimulator [42,43].

In addition, JM-2 may protect the heart by regulating other signaling pathways. For example, RNA-seq analysis showed that JM-2 may also potentially regulate IL-17, PI3K-Akt, and TNF signaling pathways. The IL-17 signaling pathway is a potent proinflammatory cytokine that participates in DCM. Li et al. showed that knockout of IL-17 attenuated ventricular arrhythmia in STZ-induced diabetic mice by inhibiting NF-κB[44]. The NF-κB signaling pathway is downstream of IL-17A, which regulates many inflammatory cytokines[45,46]. The inhibition of IL-17 can also alleviate cardiac fibrosis and dysfunction in STZ-induced diabetes [47]. Our pathway enrichment analysis showed that differentially expressed proteins (DEPs) were significantly enriched in the IL-17 signaling pathway, such as Lcn2, Ptgs2, Mmp3, and Mapk10. Lipocalin-2 (LCN2) is a downstream protein of the IL-17 pathway that is activated by IL-17[46]. Lipocalin-2 is neutrophil gelatinase-associated lipocalin, which is an attractive biomarker of inflammation and infection[48]. In T2DM, increased LCN2 expression favors inflammation via recruitment of inflammatory cells. Thus, we hypothesized that JM-2 may alleviate inflammation by affecting LCN2 levels in the serum of diabetic mice. Overall, inhibition of IL-17 may be a potential therapy for JM-2. Additionally, the PI3K-Akt signaling pathway is required for metabolism, and its imbalance leads to the development of diabetes mellitus[49]. Ren et al. showed that curcumin plays a role in DCM through the PI3K-Akt signaling pathway[50]. In summary, the curcumin analog JM-2 can alleviate inflammation by regulating the PI3K-Akt signaling pathway.

In conclusion, we present a comprehensive study that identified the therapeutic role of curcumin derivative JM-2 in DCM by inhibiting cardiac inflammation and fibrosis. Using type 1 and type 2 diabetes models, we showed that HG-induced inflammatory responses in cardiomyocytes can be completely mitigated by JM-2 treatment. Mechanistically, JM-2 exhibits anti-inflammatory and antifibrotic effects by inhibiting the NF-κB signaling pathway. Collectively, these studies clearly show an important therapeutic role for JM-2 in DCM and suggest that JM-2 could potentially be applied for therapy.

Author contributions

Guang Liang and Wu Luo contributed to the literature search and study design. Minxiu Wang participated in the drafting of the article. Minxiu Wang, Leiming Jin, Qianhui Zhang, Weiwei Zhu, Hanghui He, Shuaijie Lou carried out the experiments. Wu Luo and Xue Han revised the manuscript. Minxiu Wang and Wu Luo contributed to data collection and analysis.

CRediT authorship contribution statement

Guang Liang and Wu Luo contributed to the literature search and study design. Minxiu Wang participated in the drafting of the article. Minxiu Wang, Leiming Jin, Qianhui Zhang, Weiwei Zhu, Hanghui He, Shuaijie Lou carried out the experiments. Wu Luo and Xue Han revised the manuscript. Minxiu Wang and Wu Luo contributed to data collection and analysis. All authors have read and approved the final manuscript. All authors contributed to data analysis, drafting or revising the article, agreed on the journal to which the article will be submitted, gave final approval of the version to be published, and agreed to be accountable for all aspects of the work.

Conflict of interest statement

The authors declare that they have no conflict of interest.

Data Availability

No data was used for the research described in the article.

Acknowledgments

This study was supported by the National Natural Science Foundation of China (21961142009 to G.L.), Zhejiang Provincial Key Scientific Project (2021C03041 to G.L.), and the Natural Science Foundation of Zhejiang Province (LGJ18H310002 to X.H.).

Supplementary material

Supplemental information includes 5 figures and 1 tables. All the other data are available from the authors on request.

Appendix A. Supporting information

Supplementary data associated with this article can be found in the online version at doi:10.1016/j.biopha.2022.113590.

References

[1] G. Jia, M.A. Hill, J.R. Sowers, Diabetic cardiomyopathy: an update of mechanisms contributing to this clinical entity, Circ. Res 122 (4) (2018) 624–638.
[2] X. Cai, X. Liu, L. Sun, Y. He, S. Zheng, Y. Zhang, Y. Huang, Prediabetes and the risk of heart failure: a meta-analysis, Diabetes Obes. Metab. 23 (8) (2021) 1746–1753.
[3] L. Mai, W. Wen, M. Qiu, X. Liu, L. Sun, H. Zheng, X. Cai, Y. Huang, Association between prediabetes and adverse outcomes in heart failure, Diabetes Obes. Metab. 23 (11) (2021) 2476–2483.

[4] H. Zheng, H. Zhu, X. Liu, X. Huang, A. Huang, Y. Huang, Mitophagy in diabetic cardiomyopathy: roles and mechanisms, Front Cell Dev. Biol. 9 (2021), 750382.
[5] G. Murtaza, H.U.H. Virk, M. Khalid, C.J. Lavie, H. Ventura, D. Mukherjee, V. Ramu, S. Bhogal, G. Kumar, M. Shanmugasundaram, T.K. Paul, Diabetic cardiomyopathy - a comprehensive updated review, Prog. Cardiovasc Dis. 62 (4) (2019) 315–326.
[6] P. Ramesh, J.L. Yeo, E.M. Brady, G.P. McCann, Role of inflammation in diabetic cardiomyopathy, Ther. Adv. Endocrinol. Metab. 13 (2022), 20420188221083530.
[7] G. Frati, L. Schirone, I. Chimenti, D. Yee, G. Biondi-Zoccai, M. Volpe, S. Sciarretta, An overview of the inflammatory signalling mechanisms in the myocardium underlying the development of diabetic cardiomyopathy, Cardiovasc Res 113 (4) (2017) 378–388.
[8] A.B. Kunnumakkara, D. Bordoloi, G. Padmavathi, J. Monisha, N.K. Roy, S. Prasad, B.B. Aggarwal, Curcumin, the golden nutraceutical: multitargeting for multiple chronic diseases, Br. J. Pharm. 174 (11) (2017) 1325–1348.
[9] H. Li, A. Sureda, H.P. Devkota, V. Pittala, D. Barreca, A.S. Silva, D. Tewari, S. Xu, S. M. Nabavi, Curcumin, the golden spice in treating cardiovascular diseases, Biotechnol. Adv. 38 (2020), 107343.
[10] F. Pivari, A. Mingione, C. Brasacchio, L. Soldati, Curcumin and Type 2 Diabetes Mellitus: Prevention and Treatment, Nutrients 11 (8) (2019).
[11] Y. Chen, R. Wu, W. Chen, Y. Liu, X. Liao, B. Zeng, G. Guo, F. Lou, Y. Xiang, Y. Wang, X. Wang, Curcumin prevents obesity by targeting TRAF4-induced ubiquitylation in m(6) A-dependent manner, EMBO Rep. 22 (5) (2021), e52146.
[12] A. Giordano, G. Tommonaro, Curcumin and Cancer, Nutrients 11 (10) (2019).
[13] F. Di Meo, S. Margarucci, U. Galderisi, S. Crispi, G. Peluso, Curcumin, Gut Microbiota, and Neuroprotection, Nutrients 11 (10) (2019).
[14] C. Tang, L. Li, J. Shi, D. Wu, M. Wang, Y. Wu, X. Yuan, Curcumin in age-related diseases, Pharmazie 75 (11) (2020) 534–539.
[15] K. Morshedi, S. Borran, M.S. Ebrahimi, M.J. Masoud Khooy, Z.S. Seyedi, A. Amiri, M. Abbasi-Kolli, M. Fallah, H. Khan, A. Sahebkar, H. Mirzaei, Therapeutic effect of curcumin in gastrointestinal cancers: a comprehensive review, Phytother. Res 35 (9) (2021) 4834–4897.
[16] F. Pourhabibi-Zarandi, S. Shojaei-Zarghani, M. Rafraf, Curcumin and rheumatoid arthritis: a systematic review of literature, Int J. Clin. Pr. 75 (10) (2021), e14280.
[17] W. Yu, J. Wu, F. Cai, J. Xiang, W. Zha, D. Fan, S. Guo, Z. Ming, C. Liu, Curcumin alleviates diabetic cardiomyopathy in experimental diabetic rats, PLoS One 7 (12) (2012), e52013.
[18] J. Epstein, I.R. Sanderson, T.T. Macdonald, Curcumin as a therapeutic agent: the evidence from in vitro, animal and human studies, Br. J. Nutr. 103 (11) (2010) 1545–1557.
[19] A. Shehzad, G. Rehman, Y.S. Lee, Curcumin in inflammatory diseases, Biofactors 39 (1) (2013) 69–77.
[20] P. Anand, A.B. Kunnumakkara, R.A. Newman, B.B. Aggarwal, Bioavailability of curcumin: problems and promises, Mol. Pharm. 4 (6) (2007) 807–818.
[21] K. Shimizu, Y. Sunagawa, M. Funamoto, H. Wakabayashi, M. Genpei, Y. Miyazaki, Y. Katanasaka, N. Sari, S. Shimizu, A. Katayama, H. Shibata, Y. Iwabuchi, H. Kakeya, H. Wada, K. Hasegawa, T. Morimoto, The synthetic curcumin analogue GO-Y030 effectively suppresses the development of pressure overload-induced heart failure in mice, Sci. Rep. 10 (1) (2020) 7172.
[22] Y. Pan, Y. Wang, Y. Zhao, K. Peng, W. Li, Y. Wang, J. Zhang, S. Zhou, Q. Liu, X. Li, L. Cai, G. Liang, Inhibition of JNK phosphorylation by a novel curcumin analog prevents high glucose-induced inflammation and apoptosis in cardiomyocytes and the development of diabetic cardiomyopathy, Diabetes 63 (10) (2014) 3497–3511.
[23] L. Ye, X. Chen, M. Wang, L. Jin, Z. Zhuang, D. Yang, X. Guan, A.V. Samorodov, V. N. Pavlov, N. Chattipakorn, J. Feng, Y. Wang, W. Luo, G. Liang, Curcumin analogue C66 attenuates obesity-induced myocardial injury by inhibiting JNK-mediated inflammation, Biomed. Pharm. 143 (2021), 112121.
[24] N. Zhang, Y. Zhang, H. Qian, S. Wu, L. Cao, Y. Sun, Selective targeting of ubiquitination and degradation of PARP1 by E3 ubiquitin ligase WWP2 regulates isoproterenol-induced cardiac remodeling, Cell Death Differ. 27 (9) (2020) 2605–2619.
[25] A. Heydemann, An overview of murine high fat diet as a model for type 2 diabetes mellitus, J. Diabetes Res. 2016 (2016), 2902351.
[26] V. Kandalam, R. Basu, T. Abraham, X. Wang, P.D. Soloway, D.M. Jaworski, G. Y. Oudit, Z. Kassiri, TIMP2 deficiency accelerates adverse post-myocardial infarction remodeling because of enhanced MT1-MMP activity despite lack of MMP2 activation, Circ. Res. 106 (4) (2010) 796–808.
[27] H.K. Gaggin, J.L. Januzzi Jr., Biomarkers and diagnostics in heart failure, Biochim Biophys. Acta 1832 (12) (2013) 2442–2450.
[28] K. Kuwahara, The natriuretic peptide system in heart failure: diagnostic and therapeutic implications, Pharm. Ther. 227 (2021), 107863.
[29] M.Y. Donath, C.A. Dinarello, T. Mandrup-Poulsen, Targeting innate immune mediators in type 1 and type 2 diabetes, Nat. Rev. Immunol. 19 (12) (2019) 734–746.
[30] E. Panzhinskiy, R. Bashir, D. Bagchi, S. Nair, Effect of curcumin and alpha-lipoic acid in attenuating weight gain and adiposity, J. Am. Coll. Nutr. 38 (6) (2019) 493–498.
[31] N. Baziar, M. Parohan, The effects of curcumin supplementation on body mass index, body weight, and waist circumference in patients with nonalcoholic fatty liver disease: a systematic review and dose-response meta-analysis of randomized controlled trials, Phytother. Res 34 (3) (2020) 464–474.
[32] F. Zou, L. Wang, H. Liu, W. Wang, L. Hu, X. Xiong, L. Wu, Y. Shen, R. Yang, Sophocarpine suppresses nf-kappab-mediated inflammation both in vitro and in vivo and inhibits diabetic cardiomyopathy, Front Pharm. 10 (2019) 1219.
[33] X.M. Ren, G.F. Zuo, W. Wu, J. Luo, P. Ye, S.L. Chen, Z.Y. Hu, Atorvastatin alleviates experimental diabetic cardiomyopathy by regulating the GSK-3beta-PP2Ac-NF-kappaB signaling axis, PLoS One 11 (11) (2016), e0166740.
[34] S.G. Tang, X.Y. Liu, J.M. Ye, T.T. Hu, Y.Y. Yang, T. Han, W. Tan, Isosteviol ameliorates diabetic cardiomyopathy in rats by inhibiting ERK and NF-kappaB signaling pathways, J. Endocrinol. 238 (1) (2018) 47–60.
[35] A. Ukil, S. Maity, S. Karmakar, N. Datta, J.R. Vedasiromoni, P.K. Das, Curcumin, the major component of food flavour turmeric, reduces mucosal injury in trinitrobenzene sulphonic acid-induced colitis, Br. J. Pharm. 139 (2) (2003) 209–218.
[36] Y. Wang, Q. Tang, P. Duan, L. Yang, Curcumin as a therapeutic agent for blocking NF-kappaB activation in ulcerative colitis, Immunopharmacol. Immunotoxicol. 40 (6) (2018) 476–482.
[37] H. Zhu, X. Wang, X. Wang, B. Liu, Y. Yuan, X. Zuo, Curcumin attenuates inflammation and cell apoptosis through regulating NF-kappaB and JAK2/STAT3 signaling pathway against acute kidney injury, Cell Cycle 19 (15) (2020) 1941–1951.
[38] J. Zhang, Y. Zheng, Y. Luo, Y. Du, X. Zhang, J. Fu, Curcumin inhibits LPS-induced neuroinflammation by promoting microglial M2 polarization via TREM2/ TLR4/ NF-kappaB pathways in BV2 cells, Mol. Immunol. 116 (2019) 29–37.
[39] J. Chen, L. Zhang, Y. Shu, L. Chen, M. Zhu, S. Yao, J. Wang, J. Wu, G. Liang, H. Wu, W. Li, Curcumin Analogue CA15 Exhibits Anticancer Effects on HEp-2 Cells via Targeting NF-kappaB, Biomed. Res Int 2017 (2017), 4751260.
[40] B. Dong, D. Qi, L. Yang, Y. Huang, X. Xiao, N. Tai, L. Wen, F.S. Wong, TLR4 regulates cardiac lipid accumulation and diabetic heart disease in the nonobese diabetic mouse model of type 1 diabetes, Am. J. Physiol. Heart Circ. Physiol. 303 (6) (2012) H732–H742.
[41] Z. Wang, Z. Chen, B. Li, B. Zhang, Y. Du, Y. Liu, Y. He, X. Chen, Curcumin attenuates renal interstitial fibrosis of obstructive nephropathy by suppressing epithelial-mesenchymal transition through inhibition of the TLR4/NF-small ka, CyrillicB and PI3K/AKT signalling pathways, Pharm. Biol. 58 (1) (2020) 828–837.
[42] C. Lin, Y. Guo, Y. Xia, C. Li, X. Xu, T. Qi, F. Zhang, M. Fan, G. Hu, H. Zhao, H. Zhao, R. Liu, E. Gao, W. Yan, L. Tao, FNDC5/Irisin attenuates diabetic cardiomyopathy in a type 2 diabetes mouse model by activation of integrin alphaV/beta5-AKT signaling and reduction of oxidative/nitrosative stress, J. Mol. Cell Cardiol. 160 (2021) 27–41.
[43] T. Ma, X. Huang, H. Zheng, G. Huang, W. Li, X. Liu, J. Liang, Y. Cao, Y. Hu, Y. Huang, SFRP2 improves mitochondrial dynamics and mitochondrial biogenesis, oxidative stress, and apoptosis in diabetic cardiomyopathy, Oxid. Med Cell Longev. 2021 (2021), 9265016.
[44] D.S. Li, G.L. Xue, J.M. Yang, C.Z. Li, R.X. Zhang, T. Tian, Z. Li, K.W. Shen, Y. Guo, X.N. Liu, J. Wang, Y.J. Lu, Z.W. Pan, Knockout of interleukin-17A diminishes ventricular arrhythmia susceptibility in diabetic mice via inhibiting NF-kappaB-mediated electrical remodeling, Acta Pharm. Sin. 43 (2) (2022) 307–315.
[45] D.K. McDaniel, K. Eden, V.M. Ringel, I.C. Allen, Emerging roles for noncanonical nf-kappab signaling in the modulation of inflammatory bowel disease pathobiology, Inflamm. Bowel Dis. 22 (9) (2016) 2265–2279.
[46] N. Shembade, E.W. Harhaj, IKKi: a novel regulator of Act1, IL-17 signaling and pulmonary inflammation, Cell Mol. Immunol. 8 (6) (2011) 447–449.
[47] E. Yue, Y. Yu, X. Wang, B. Liu, Y. Bai, B. Yang, Anthocyanin protects cardiac function and cardiac fibroblasts from high-glucose induced inflammation and myocardial fibrosis by inhibiting IL-17, Front Pharm. 11 (2020), 593633.
[48] A.R. Moschen, T.E. Adolph, R.R. Gerner, V. Wieser, H. Tilg, Lipocalin-2: a master mediator of intestinal and metabolic inflammation, Trends Endocrinol. Metab. 28 (5) (2017) 388–397.
[49] X. Huang, G. Liu, J. Guo, Z. Su, The PI3K/AKT pathway in obesity and type 2 diabetes, Int J. Biol. Sci. 14 (11) (2018) 1483–1496.
[50] B.C. Ren, Y.F. Zhang, S.S. Liu, X.J. Cheng, X. Yang, X.G. Cui, X.R. Zhao, H. Zhao, M. F. Hao, M.D. Li, Y.Y. Tie, L. Qu, X.Y. Li, Curcumin alleviates oxidative stress and inhibits apoptosis in diabetic cardiomyopathy via Sirt1-Foxo1 and PI3K-Akt signalling pathways, J. Cell Mol. Med 24 (21) (2020) 12355–12367.